ACS APPLIED MATERIALS & INTERFACES

Research Article

www.acsami.org

Modulation of Human Mesenchymal Stem Cell Behavior on Ordered Tantalum Nanotopographies Fabricated Using Colloidal Lithography and Glancing Angle Deposition

Peng-Yuan Wang,[†,‡] Dines T. Bennetsen,[§] Morten Foss,[§] Thomas Ameringer,[†] Helmut Thissen,[‡] and Peter Kingshott*[,†]

[†]Industrial Research Institute Swinburne (IRIS) and Department of Chemistry and Biotechnology, Swinburne University of Technology, Hawthorn, 3122 Victoria, Australia

[‡]CSIRO Manufacturing Flagship, Bayview Avenue, Clayton, 3168 Victoria, Australia

[§]Interdisciplinary Nanoscience Center (iNANO), Faculty of Science, Aarhus University, Ny Munkegade, 8000 Aarhus C, Denmark

Supporting Information

ABSTRACT: Ordered surface nanostructures have attracted much attention in biotechnology and biomedical engineering because of their potential to modulate cell−surface interactions in a controllable manner. However, the ability to fabricate large area ordered nanostructures is limited because of high costs and low speed of fabrication. Here, we have fabricated ordered nanostructures with large surface areas (1.5 × 1.5 cm^2) using a combination of facile techniques including colloidal self-assembly, colloidal lithography and glancing angle deposition (GLAD). Polystyrene (722 nm) colloids were self-assembled into a hexagonally close-packed (hcp) crystal array at the water−air interface, transferred on a biocompatible tantalum (Ta) surface and used as a mask to generate an ordered Ta pattern. The Ta was deposited by sputter coating through the crystal mask creating approximately 60-nm-high feature sizes. The feature size was further increased by approximately 200-nm-height respectively using GLAD, resulting in the fabrication of four different surfaces (FLAT, Ta60, GLAD100, and GLAD200). Cell adhesion, proliferation, and osteogenic differentiation of primary human adipose-derived stem cells (hADSCs) were studied on these ordered nanostructures for up to 2 weeks. Our results suggested that cell spreading, focal adhesion formation, and filopodia extension of hADSCs were inhibited on the GLAD surfaces, while the growth rate was similar between each surface. Immunostaining for type I collagen (COL1) and osteocalcin (OC) showed that there was higher osteogenic components deposited on the GLAD surfaces compared to the Ta60 and FLAT surfaces after 1 week of osteogenic culture. After 2 weeks of osteogenic culture, alkaline phosphatase (ALP) activity and the amount of calcium was higher on the GLAD surfaces. In addition, osteoblast-like cells were confluent on Ta60 and FLAT surfaces, whereas the GLAD surfaces were not fully covered suggesting that the cell−cell interactions are stronger than cell−substrate interactions on GLAD surfaces. Visible extracellular matrix deposits decorated the porous surface can be found on the GLAD surfaces. Depth profiling of surface components using a new Ar cluster source and X-ray photoelectron spectroscopy (XPS) showed that deposited extracellular matrix on GLAD surfaces is rich in nitrogen. The fabricated ordered surface nanotopographies have potential to be applied in diverse fields, and demonstrate that the behavior of human stem cells can be directed on these ordered nanotopographies, providing new knowledge for applications in biomaterials and tissue engineering.

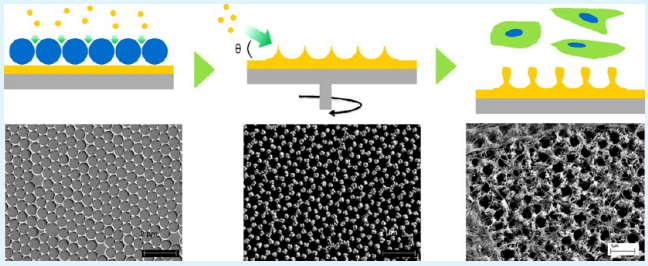

KEYWORDS: *colloidal self-assembly, glancing angle deposition, ordered topography, human adipose-derived stem cells, osteogenic differentiation*

1. INTRODUCTION

It has been recognized that the symmetry and feature size of surface topographies are able to determine initial cell-surface interactions and subsequent cell fate on artificial materials that are used as biomaterials and in tissue engineering applications.[1,2] Controlling cell behavior including adhesion, migration, proliferation, differentiation, and even apoptosis by controlling feature sizes, spatial distributions, and the symmetry of topographies or cell-binding ligands at biomaterial surfaces has the potential to provide a cost-effective tool for biomedical engineers. In addition, exploration of cellular responses to such advanced artificial substrates enhances the basic understanding of complicated cell-extracellular matrix (ECM) interactions, which is difficult to study *in vivo*.

Received: January 6, 2015
Accepted: February 9, 2015
Published: February 9, 2015

DOI: 10.1021/acsami.5b00107
ACS Appl. Mater. Interfaces 2015, 7, 4979−4989

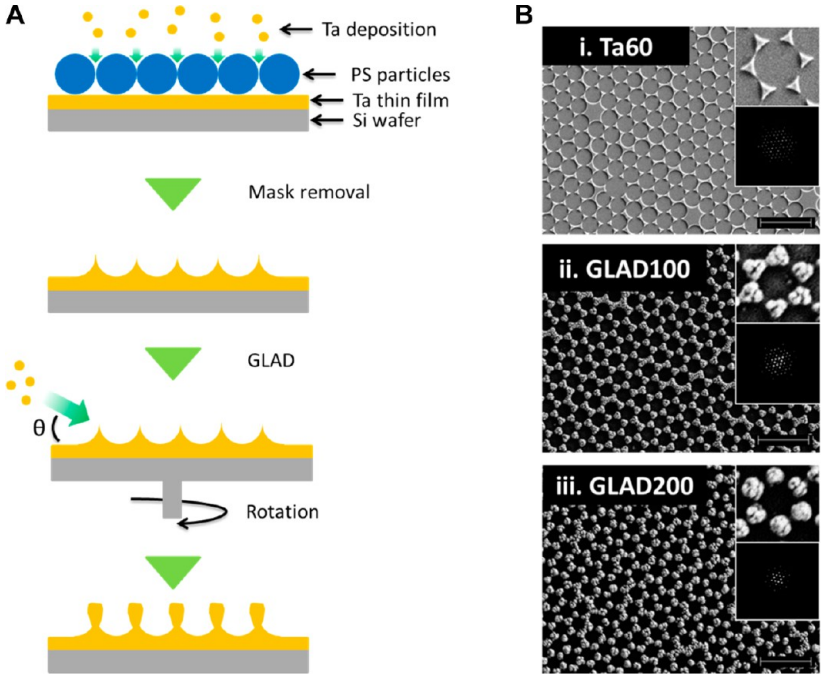

Figure 1. Fabrication of ordered Ta nanotopographies using a combination of colloidal self-assembly, colloidal lithography, and glancing angle deposition (GLAD) techniques. (A) The procedure of assembly of 722 nm PS colloids, sputter coating of 60 nm Ta (Ta60), mask removal, and GLAD of Ta for increasing of feature heights (GLAD100 or GLAD200). (B) Scanning electron micrographs (SEMs) of (i) Ta60, (ii) GLAD100, and (iii) GLAD200. The inserted images showed a single unit of the features (upper), and image analysis using Fast Fourier Transform (FFT; lower). Scale bar = 2 μm.

A number of methods such as photolithography, e-beam lithography, and focused ion beam lithography have been developed for the fabrication of various surface patterns including pits, grooves, pillars, etc., for cell culture.[3−6] Although lithographic approaches using high energy particles, such as photons, electrons, and ions, are well-developed, they also suffer from limitations that prevent them from being used frequently in bench-scale experiments, particularly in the biological and chemical fields.[7] The disadvantages of some of these techniques are related to speed, equipment costs including maintenance, and an ability to generate relatively small patterned surface areas. Even when access to instruments is available, designing and testing new patterns can be slow. Therefore, a simple and easy approach providing access to surface nanopatterning is highly desired.

Self-assembly of spherical colloids into hexagonal close-packed (hcp) crystal monolayers has attracted much attention in the past few decades.[8,9,52] Using colloidal crystal monolayers as masks enables various surface nanostructures to be obtained including triangle textures, nanopits, and nanorods.[7,10] This approach is relatively simple. Surprisingly, however, colloidal crystal monolayers have rarely been used to fabricate ordered surface nanostructures for mammalian cell culture studies and to investigate cell−surface interactions. Two main reasons for this are (1) fabrication of colloidal crystal monolayers into large surface areas is difficult, and (2) the feature size, height, and spacing variations can be limited.

The glancing angle deposition (GLAD) method has also attracted attention due to its relative simplicity and feasibility for increasing surface feature size in the z-direction on the sub-10 nm scale.[11] By adjusting the incident angle (<10°), rotation speed, and time, columnar nanostructures are accumulated on the top of original features (seeds) due to the self-shadowing effect. Thus, the surface feature size can be readily increased vertically. Promising applications have been demonstrated for this facile approach in photonic crystals, biosensing, photovoltaics, and fuel cells.[12−15] Several recent reports have also used the GLAD technique to generate roughened surfaces for bacterial or mammalian cell culture.[16−18] In general, the results suggest that on nanoroughened GLAD surfaces, cell spreading and focal adhesion complexes are reduced, filopodia are smaller and shorter, actin filaments are impaired, and/or migration-related genes are down-regulated compared with flat control surfaces. These studies introduced the GLAD technique as a new method for the modification of biomaterial surfaces.

The aim of this study was to fabricate highly ordered, nanostructured substrates using a combination of colloidal lithography and the GLAD techniques for controlling adhesion, growth, and differentiation of human mesenchymal stem cells (hMSCs). To achieve this goal, ordered surface nanostructures covering large areas constructed by biocompatible Ta (tantalum), a promising endosseous implant coating, were fabricated using self-assembled colloids as a mask. Subsequently, the size and height of the Ta nanofeatures was then increased using the GLAD technique. Cell adhesion, proliferation, and osteogenic differentiation of human adipose-derived stem cells (hADSCs) were studied on these substrates for up to 2 weeks. This is the first study to use colloidal self-assembly, colloidal lithography, and GLAD technique to generate centimeter-size ordered nanostructures for human MSC culture. Our results enhance the understanding of topographic effects on stem cell response and potentially facilitate the development of new biomaterial surfaces for bone tissue engineering.

2. MATERIALS AND METHODS

2.1. Materials. Polystyrene (PS) particles with a diameter of 722 ± 40 nm (10% w/v) were purchased from Microparticles GmbH (Berlin,

DOI: 10.1021/acsami.5b00107
ACS Appl. Mater. Interfaces 2015, 7, 4979−4989

Germany). Si wafers (P/Bor ⟨100⟩, 10−20 Ω cm) were purchased from Si-Mat (Kaufering, Germany). Titanium (Ti; 99.99%, cat#LS377240) and tantalum (Ta; 99.99%, cat#LS387734 MKS), sources for evaporation, were purchased from Goodfellow (Huntingdon, England). Targets for sputtering (Ti and Ta) with a purity of 99.9% were purchased from CERAC (Milwaukee, WI, USA).

Primary human adipose-derived stem cells (hADSCs, cat#PCS-500−011), stem cell basal medium (cat#PCS-500−030), stem cell growth kit (cat#PCS-500−040), D-PBS (cat#30−2200), trypsin-EDTA (cat#PCS-999−003), trypsin neutralizing solution (PCS-999−004), and the osteocyte differentiation tool (cat#PCS-500−052) were purchased from American Type Culture Collection (ATCC, Manassas, VA, USA). Antibiotic−antimycotic solution (cat#15240−112) and phosphate buffered saline (PBS, cat#AM9625) were purchased from Invitrogen (Grand Island, NY, USA). Phalloidin−tetramethylrhodamine B isothiocyanate (phalloidin-TRITC, cat#P1951), 4,6-diamidino-2-phenylindole (DAPI, cat#D9542), paraformaldehyde (PFA, cat#158127), bovine serum albumin (BSA, cat#A7906), monoclonal antivinculin antibody produced in mouse (cat#V9264), monoclonal antitype I collagen antibody produced in mouse (cat# C2456), antimouse IgG (whole molecule)-FITC antibody produced in goat (cat#F2012), antimouse IgG (whole molecule)-TRITC antibody produced in goat (cat# T5393), and sodium dodecyl sulfate (SDS, cat#L3771) were purchased from Sigma-Aldrich (St. Louis, MO, USA). Other chemicals used in this study were purchased from Sigma-Aldrich unless specified otherwise.

2.2. Colloidal Self-Assembly and Substrate Preparation. Highly ordered Ta nanotopographies were fabricated using the colloidal lithography and glancing angle deposition (GLAD) techniques (Figure 1A). Colloids were self-assembled into crystal monolayers at the liquid−air interface using a method similar to previous reports,[19,20] and then transferred onto a flat Ta surface. Briefly, Si wafers were sputter-coated with 4 nm titanium (Ti) and then 100 nm tantalum (Ta) with deposition rates of 0.4−0.9 nm/sec (sample referred to as FLAT). Deposition was performed at a chamber pressure of 10^{-7} mbar at ambient temperature. FLAT samples were then cut into 1 cm^2 pieces and subsequently cleaned by 20 min sonication in ethanol and then Milli-Q water, followed by 20 min UV/ozone treatment. PS particle suspensions (722 nm) were mixed with ethanol (2:1 v/v). The particle mixture was then carefully dispersed onto the surface of Milli-Q water in a plastic dish. 2% (v/v) SDS solution was added to help particles self-assemble at the water surface. Once particles assembled into a coherent colloidal crystal with sufficient coverage the crystal monolayer was transferred to the Ta substrates. After colloidal mask formation, a Ti adhesion layer (50 s deposition time; approximately 4 nm thickness) followed by a Ta layer (500 s deposition time; approximately 60 nm thickness) were evaporated onto the Si wafer through the colloidal masks using a customized deposition system at the Institute of Physics and Astronomy (Aarhus University). After particles were removed by sonication in Milli-Q water, ordered Ta patterns with triangular shape were formed (sample referred to as Ta60). GLAD was then performed using the same sputtering equipment and conditions with an incidence angle of 5°. The Ta60 samples were coated either for 140 or 280 s, giving two GLAD samples with an extra height of 100 nm (GLAD100) or 200 nm (GLAD200), respectively.

2.3. Surface Characterization. Surface topography was characterized using scanning electron microscopy (SEM) and atomic force microscopy (AFM). SEM images were obtained using a Magellan XHR (FEI, The Netherlands) instrument. Images were acquired in high vacuum using a voltage of 5 kV and a working distance of approximately 5 mm. AFM images were acquired using a Nanowizard 2 (JPK, Berlin, Germany) instrument with a silicon nitride cantilever (Olympus AC series with typical spring constant 26 N/m and typical tip radius of 7 nm). All images were acquired in air and in "tapping mode". Images were analyzed using the JPKSPM Data Processing software (JPK). Surface wettability of substrates was determined using a water contact angle (WCA) goniometer (KSV instruments Ltd., Finland) and the static sessile drop method. A drop of Milli-Q water (0.5 μL) was deposited on substrate surfaces and six spots were analyzed (n = 6). The symmetry of the surface topography was characterized using Fast Fourier Transform (FFT) analysis and ImageJ software.

2.4. Stem Cell Culture and Analysis. Prior to cell seeding, substrates were sterilized using 70% ethanol and rinsed three times with PBS. Human adipose-derived stem cells (hADSCs) were seeded with a cell density of 1×10^4 cells/cm^2 for cell growth, and 2×10^4 cells/cm^2 for osteogenic differentiation. Cell morphology, density and spreading area were characterized after 24 h, while cell growth was determined after 1, 3, and 6 days using field emission SEM (FE-SEM; ZEISS SUPRA 40 VP, Carl Zeiss, Germany) and inverted fluorescence microscopy (Eclipse Ti-E, Nikon, Japan). At each time point, samples were rinsed with PBS twice, fixed with 4% PFA, permeated with 0.2% PBST (PBS with Triton X-100), and blocked with 1% BSA. Cell nuclei and F-actin were stained by DAPI (100 nM) and Phalloidin-TRITC (500 nM), respectively, for 1 h. Cell density and cell spreading area was determined by counting nuclei and quantifying F-actin staining, respectively, from 4× fluorescence images using ImageJ software. Three parallel experiments were carried out with 6 images captured at each time point (n = 6). Focal adhesions of hADSCs were determined by staining of vinculin using an antivinculin primary antibody (1:100 dilution in PBS), followed by an FITC-conjugated secondary antibody (1:100 dilution in PBS) at room temperature for 1 h, respectively. Focal adhesions were imaged using confocal laser scanning microscopy (A1Rsi, Nikon, Japan).

2.5. Osteogenic Differentiation and Analysis. After 2 day incubation of hADSCs, the culture medium was changed to osteogenic medium following the supplier's instructions (ATCC, USA). Osteoblasts-like cells were characterized after 1 and 2 weeks by means of alkaline phosphatase (ALP) activity as well as calcium deposition. ALP activity was assayed by determining the release of p-nitrophenyl (PNP) from p-nitrophenyl phosphate (PNPP) according to a previous described procedure.[21] Briefly, 25 μL cell lysate in 0.2% PBST was reacted with 100 μL PNPP (1 mg/mL, cat#0942, Sigma) in AMP buffer (0.5 M 2-amino-2-methyl-1propanol and 2 mM $MgCl_2$, pH 10) for 30 min. The reaction was stopped by adding 0.5 N NaOH and the absorbance at 405 nm was read in an ELISA reader (FLUOstar Galaxy, BMG LABTECH, Ortenberg, Germany). A series of known concentrations of PNP were used to generate a calibration curve to determine ALP activity.

The amount of calcium deposition on surfaces was determined using a calcium assay (Arsenazo III, cat#140−20, Diagnostic Chemicals Limited, USA) according to a previously described procedure.[21] Briefly, deposited calcium in the samples was extracted in 0.6 N HCl solutions overnight at 4 °C. 100 μL of the extract was then mixed with 1 mL of calcium working solution. The absorbance at 650 nm of the generated blue-purple complex was measured using an UV−vis spectrophotometer (Cary 50 Bio, Varian, INC., Palo Alto, California). The calcium content was determined using a calibration curve generated from a series of calcium solutions with known concentrations. Both the ALP activity and the calcium content were normalized to the surface area of the substrate.

Immunostaining of type I collagen (COL1) and osteocalcin (OC) was carried out after 1 week induction culture modified according to a previous study.[22] Briefly, samples were rinsed with PBS twice, fixed with 4% PFA, permeated with 0.2% PBST (PBS with Triton X-100), and blocked with 1% BSA. For COL1, samples were incubated with mouse antitype I collagen IgG (1:100 dilution in PBS) at room temperature for 1 h, followed by incubation with FITC-conjugated antimouse IgG (1:100 dilution in PBS) at room temperature for 1 h. For OC, samples were incubated with rabbit antiosteocalcin IgG (1:100 dilution in PBS) at room temperature for 1 h, followed by incubation with TRITC-conjugated antirabbit IgG (1:100 dilution in PBS) at room temperature for 1 h. Cell nuclei were stained with 100 nM DAPI for another 1 h at room temperature.

The calcium and phosphorus content was further characterized using X-ray photoelectron spectroscopy (XPS, AXIS Nova, Kratos Analytical Ltd., Manchester, UK). Samples were fixed with 4% PFA, rinsed with DI water three times, and air-dried. The depth profile of

DOI: 10.1021/acsami.5b00107
ACS Appl. Mater. Interfaces 2015, 7, 4979−4989

surface components was obtained using the Ar Gas Cluster Ion Source (GCIS), which is optimized for depth profiling organic materials in Ar_{500} + cluster mode. In this mode, the maximal ion energy of 20 keV (HT) was used for 20 s for each layer to a total of 800 s (cluster size 500^+; 2 × 2 mm irradiation size (crater size); extractor current 25 μA; emission current 10 mA; beam monitor current 5 μA). Survey spectra (1200−0 eV; pass energy 160; 110 μm aperture (area of analysis); anode 10 mA/HT 15 kV = 150W) were used to analyze the surface elemental composition. All elements at each layer were quantified, and the concentration (%) vs time (s) was plotted.

2.6. Statistical Analysis. Statistical analysis was performed using GraphPad Instat 3.0 program (GraphPad Software, La Jolla, CA). The statistical analysis between each group was determined with one-way ANOVA and Student−Newman−Keuls multiple comparisons test. $p < 0.05$ was considered as significant difference. Quantitative analyses were done on at least 3 samples and the experiment was performed at least 3 times.

3. RESULTS

3.1. Ordered Ta Nanotopographies. Long-range ordered Ta nanostructures were fabricated using a combination of colloidal lithography and GLAD (Figure 1A). The ability to fabricate long-range ordered hexagonal-close packed (hcp) colloidal crystal masks is one of the key steps. Using a technique described in previous studies,[19,20] self-assembly of 722 nm PS particles at the water−air interfaced created a single colloidal crystal monolayer, which was then transferred to Ta-coated Si wafers (FLAT) that could subsequently be used as a mask. Triangle-shaped Ta nanostructures were then generated by deposition of Ta onto the FLAT substrates through the interstitial spaces between the colloidal particles of the mask after their removal (Figure 1B, image i). The feature size of these triangles was approximately 60 nm in height and 350 nm in length (Figure S1 in the Supporting Information), whereas the spacing was approximately 380 nm. To increase the feature size of these triangular seed structures, the GLAD technique was used. Columnar structures were developed from the seeds and their height was dependent on the coating time. Two different coating times (140 and 280 s) were chosen to obtain two different heights of GLAD generated structures. The height of the seed structures was increased by another 100 and 200 nm, respectively (GLAD100 and GLAD200) (Figure 1B, image ii and image (iii). However, a porous surface topography was generated after GLAD coating. Due to the growth of the columnar structure, the pore size was slightly decreased with an increase of deposition time. The triangular shape of the features gradually disappeared as the columnar structure grew. A dough ball-like structure was found on the GLAD200 sample. The feature size of these structures was approximately 400−450 nm, and the pore size of GLAD samples was approximately 350−400 nm. FFT analysis showed that the hcp arrangement remained on all surfaces (inserted images, Figure 1B). The surface roughness (Ra) of the Ta60, GLAD100, and GLAD200 was 13.6 ± 1.2 nm, 51.5 ± 0.3 nm, and 42.6 ± 1.0 nm, respectively, whereas it was 0.8 ± 0.3 nm on the FLAT surface (Figure 2A). The water contact angles (WCA) recorded on the Ta60, GLAD100, and GLAD200 surfaces were 81.7 ± 1.5°, 121.4 ± 7.6°, and 128.6 ± 1.3°, respectively, whereas that of the FLAT control was 55.5° ± 2.0° (Figure 2B). Thus, the surface roughness and WCA for both GLAD100 and GLAD200 were essentially the same as a result of the center of the pores being coated with longer GLAD treatment times.

3.2. Stem Cell Culture and Osteogenic Differentiation. Cell adhesion, morphology, and density of human adipose-derived stem cells (hADSCs) on each surface were characterized using confocal fluorescence microscopy and SEM after 24 h. hADSCs were fully spread and elongated with multiple thin and long protrusions on the FLAT substrate (Figure 3A). The cell morphology observed on nano-topographies was roughly similar to that on the FLAT surface, yet the number of cell protrusions and/or filopodia on GLAD100 and GLAD200 was reduced in comparison to the FLAT and Ta60 samples (from 0.7 per μm cell periphery down to 0.3 per μm cell periphery, Figure 3B). In addition, the length of the filopodia was significantly decreased after GLAD coating (from >3 μm down to <1 μm, Figure 3B). The longer cell extension indicates that mature cell adhesions were formed on FLAT and Ta60 (focal adhesions, FAs), while immature cell adhesions were on GLAD surfaces (focal contacts, FXs).[23] Vinculin staining clearly showed that this protein was aggregated at the cell protrusions and colocalized with F-actin (red) on FLAT substrates, while on the GLAD200 vinculin molecules were distributed within the cytoplasm of attached cells (Figure 4).

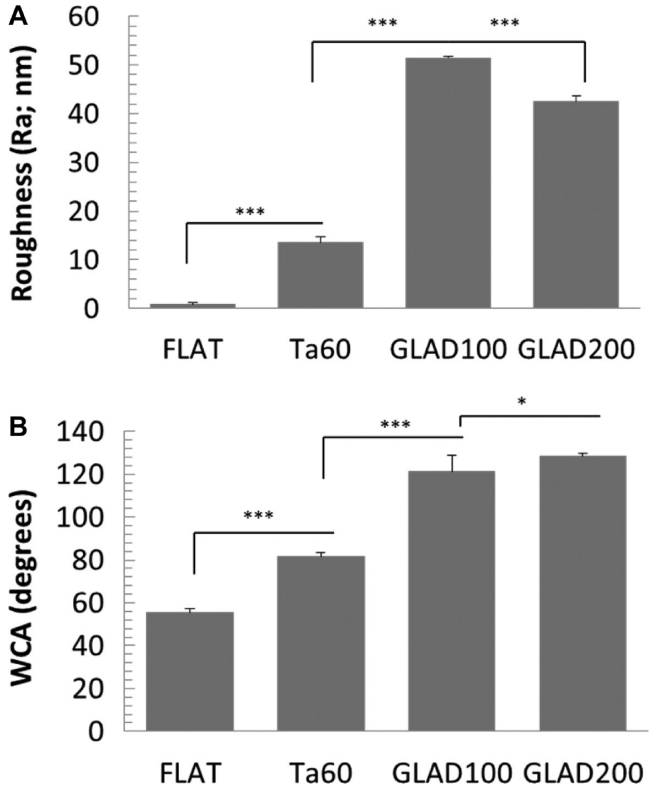

Figure 2. Surface roughness (Ra) and water contact angle (WCA) analysis. (A) Surface roughness was quantified ($n > 3$) from atomic force microscopy (AFM) images with a size of 10 × 10 μm^2. (B) WCA was quantified ($n > 6$) using sessile drop methods. Values = mean ± STDEV. * $p < 0.05$, *** $p < 0.001$.

The average cell spreading area on GLAD100 (875 ± 111 μm^2) and GLAD200 (805 ± 100 μm^2) was significantly smaller than the average area determined on Ta60 (1103 ± 122 μm^2, $p < 0.05$) and FLAT substrates (3120 ± 200 μm^2, $p < 0.001$) after 24 h (Figure 5A). After 3 day and 6 day culture, the average cell spreading area on Ta60 (1792 ± 197 μm^2 after 3 days and 1814 ± 179 μm^2 after 6 days) and FLAT surfaces (1716 ± 112 μm^2 after 3 days and 1627 ± 161 μm^2 after 6 days) was similar, while the average area determined on GLAD100 (1381 ± 79 μm^2 after 3 days and 1370 ± 76 μm^2

DOI: 10.1021/acsami.5b00107
ACS Appl. Mater. Interfaces 2015, 7, 4979−4989

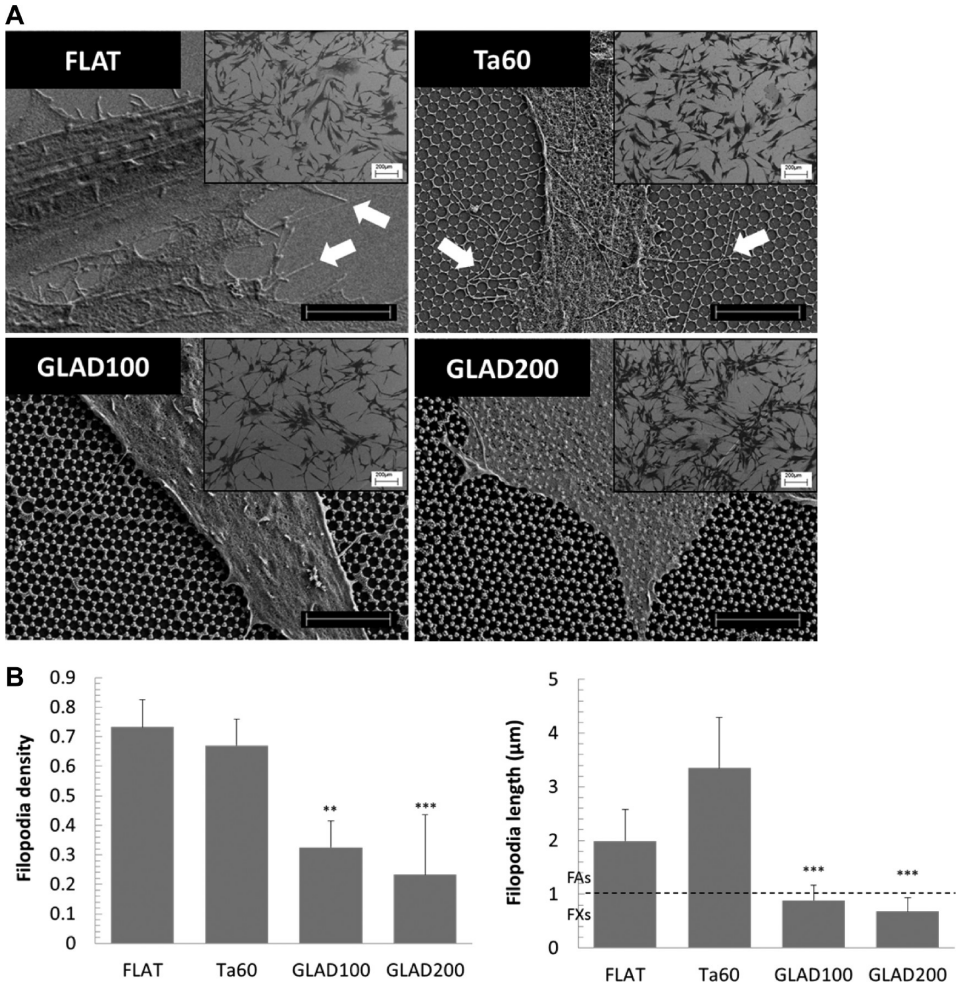

Figure 3. (A) Scanning electron micrographs (SEMs) of hADSCs on surfaces after 24 h. The inserted images (upper right corner) show a larger area of cell morphology, while the large images showed the detail of cell-surface interaction with protrusions and filopodia. The arrows indicated the thin and long cell protrusions on FLAT and Ta60 surfaces. Scale bar = 5 μm in the images, and 200 μm in the inserted images. (B) Quantitative data of filopodia density (number per μm of cell periphery) and length (μm). The dash line indicates the boundary of focal adhesions (FAs) and focal contacts (FXs). Values = mean ± STDEV. ** $p < 0.01$ and *** $p < 0.001$ vs FLAT surface.

after 6 days) and GLAD200 surfaces (1421 ± 121 μm^2 after 3 days and 1565 ± 97 μm^2 after 6 days) was significantly lower.

Cell attachment density on each surface was similar after 24 h culture, where on FLAT, Ta60, GLAD100, and GLAD200, 5303 ± 577 cells/cm^2, 6677 ± 2272 cells/cm^2, 6155 ± 1186 cells/cm^2, and 5344 ± 920 cells/cm^2 were attached, respectively (Figure 5B). After 6 days of culture, the cell density on GLAD100 and GLAD200 was 6.6 ± 0.9 × 10^4 cells/cm^2 and 6.1 ± 0.4 × 10^4 cells/cm^2 which was approximately 18% higher compared to Ta60 (5.2 ± 0.5 × 10^4 cells/cm^2, $p < 0.01$ compared to both GLAD surfaces) and the FLAT control (5.5 ± 0.6 × 10^4 cells/cm^2, $p < 0.05$ compared to both GLAD surfaces, Figure 5B).

For the osteogenic differentiation study, the culture medium was replaced by an osteogenic medium after 2 days. ALP activity on each surface was then quantified after time intervals of 3, 7, and 14 days (Figure 6A). The ALP activity was the highest on the GLAD100 sample and this was significantly higher than the activity observed on the FLAT surface over the 2 week culture period. The amount of calcium was also quantified after 3, 7, and 14 days, and was the highest on GLAD200 after 2 weeks of culture. Calcium deposition on TCPS was the highest after 3 and 7 days, but not after 14 days (Figure 6B).

Immunostaining for COL1 and OC deposition by the osteogenic hADSCs after 1 week showed that COL1 and OC were strongly expressed on GLAD200 surfaces but weakly expressed on other surfaces (Figure 7). COL1 was found as condensed deposits within some cells (arrows, Figure 7), whereas OC was uniformly distributed on the cells. Because of incomplete cell coverage some of the underlying GLAD100 and GLAD200 surfaces were exposed after 2 weeks of osteogenic culture. Within these exposed areas visible extracellular matrix (ECM) was found deposited on the surface (Figure 8A, image iii and iv). These ECM components were rarely found on the Ta60 and FLAT surfaces (Figure 8A, image i and ii). To further confirm the surface components after osteogenic differentiation, XPS chemical depth profiling through the layers on GLAD200 (Figure 8B) and GLAD100 (Figure S2 in the Supporting Information) using an Ar cluster source was undertaken. This method has been shown to have minimal damage associated with the sputtering process and thus allows for nondestructive chemical composition determination during depth profiling.[24] Calcium (Ca 2p) and phosphorus (P 2p) were both detected on the top surface of the cell samples,

DOI: 10.1021/acsami.5b00107
ACS Appl. Mater. Interfaces 2015, 7, 4979−4989

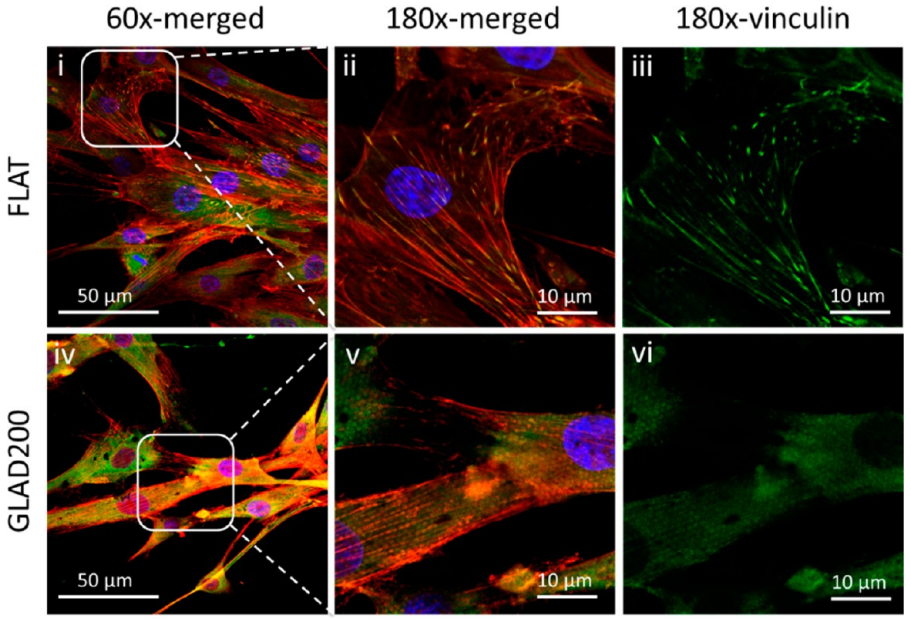

Figure 4. Confocal laser scanning microscopy of ADSCs on surfaces after 24 h. Cells on (i, ii, iii) FLAT and (iv, v, vi) GLAD200 surfaces were immunostained with 1st antivinculin and then 2nd IgG-FITC (green). F-actin and nucleus was stained using Phalloidin-TRITC (red) and DAPI (blue). The zoom-in images (ii, iii and v, vi) showed the detail of focal adhesions and cytoskeleton distribution.

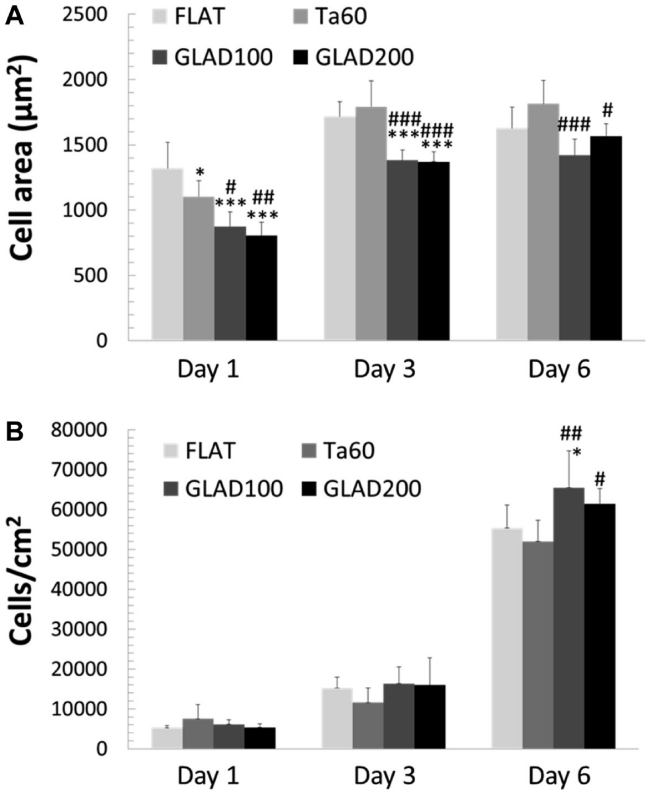

Figure 5. Cell spreading area and cell density. (A) Cell spreading area on surfaces was quantified by drawing the periphery of cells using ImageJ software. At least 50 cells were analyzed ($n > 50$) at each time point. (B) Cell density on surfaces was quantified by counting the DAPI-stained nuclei using ImageJ software. At least 6 images were analyzed ($n > 6$) at each time point. Value = mean ± STDEV. # and * indicate there is a significant difference vs FLAT and Ta60, respectively. One, two, and three symbols indicate the $p < 0.05$, 0.01, and 0.001, respectively.

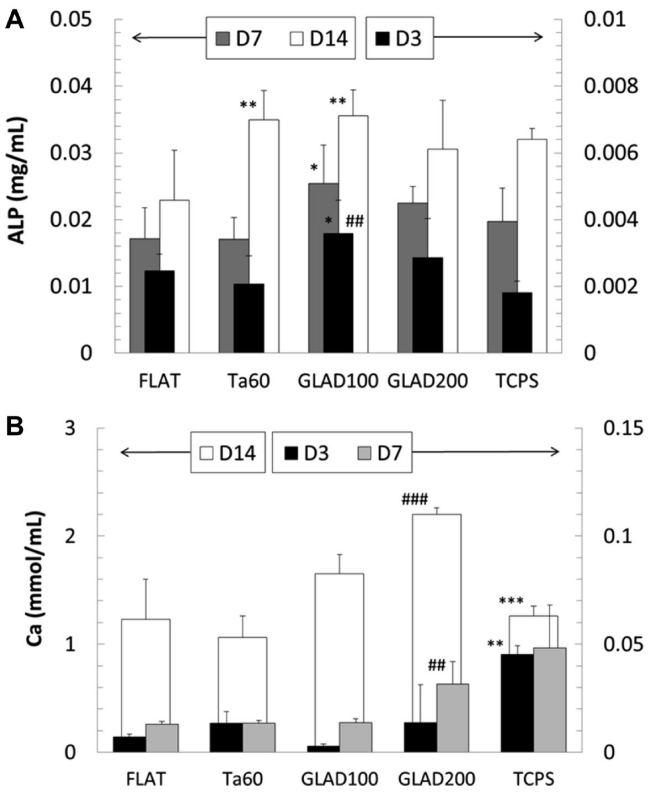

Figure 6. Alkaline phosphatase (ALP) and calcium (Ca) quantification of osteogenic differentiated hADSCs. (A) ALP synthesis and (B) Ca deposition on the surfaces by the cells were quantified with at least three samples ($n > 3$) with three independent runs of experiments. # and * indicate there is a significant difference vs FLAT and Ta60, respectively. One, two, and three symbols indicate the $p < 0.05$, 0.01, and 0.001, respectively.

which gradually decreased as the cells were etched (Figure 8C), suggesting that mineralization induced Ca and P deposition

DOI: 10.1021/acsami.5b00107
ACS Appl. Mater. Interfaces 2015, 7, 4979−4989

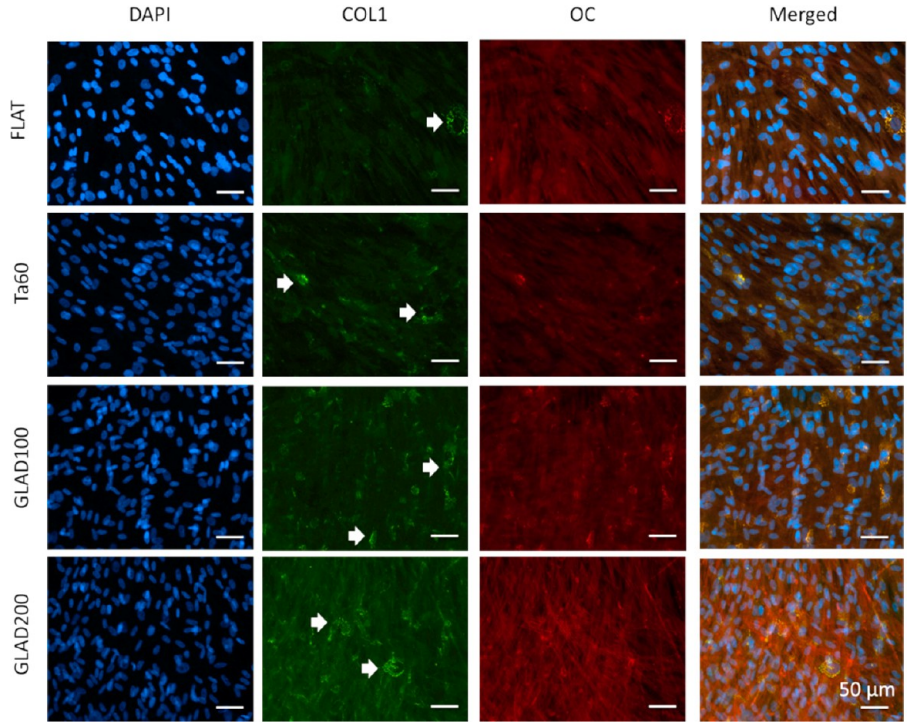

Figure 7. Immunostaining of type 1 collagen (COL1) and osteocalcin (OC) of osteogenic differentiated hADSCs after 1 week. Cells on surfaces were immunostained with 1st anti-COL1 and 1st anti-OC, and 2nd anti-COL1-FITC (green) and 2nd anti-OC-TRITC (red), respectively. Nuclei were stained using DAPI (blue). The arrows indicated condensed COL1 protein deposit.

mostly likely occurred on the cell and substrate surface rather than inside the cell and substrate. While carbon (C 1s), oxygen (O 1s), calcium (Ca 2p), and phosphorus (P 2p) were decreased, tantalum (Ta 4d) and nitrogen (N 1s) were increased with the depth increase, suggesting that the nitrogen-containing proteins and biomolecules were produced within cells or pores on substrate during osteogenic differentiation.

4. DISCUSSION

Ordered nanostructure arrays, consisting of regular nanofeatures, are useful in many fields including photonics, plasmonics, solar cells, surface-enhanced Raman scattering (SERS) substrates, photocatalysis, antireflection, and biosensors, as well as biomimetic fabrication for cell culture.[7,22,25−27] Colloidal lithography using self-assembled colloidal crystal monolayer masks is a cost-effective and versatile method to generate hexagonal close-packed (hcp), highly ordered nanotopographies, but rarely other arrangements. The ability to generate colloidal crystal masks is the key for the fabrication of ordered nanotopographies using colloidal lithography. Here we have developed a method that is able to generate monolayer colloidal crystal masks with a size of tens of cm^2 using 722 nm PS particles.[20] The mask can be readily transferred on to any material with particles of different size possible. Robust and ordered nanostructures can be generated by deposition of layers through the voids of the mask. Using the GLAD technique, various feature heights and surface roughnesses can be developed depending on the deposition time generating a porous substrate. The optical properties of the Ta60 surfaces were changed after GLAD coating. The vivid structural color can be seen on Ta60, while it cannot be seen on GLAD200. We also found that the fluorescence intensity of immunostained samples on GLAD surfaces was weaker than that on Ta60 surface, suggesting that an antireflection property was developed after GLAD coating. Although colloidal self-assembly and/or lithography and GLAD techniques have been individually explored in the literature,[26,28] studies that combine these techniques for biological applications are difficult to find. For example, the ordered nanotopographies generated by colloidal self-assembly and/or lithography has been used to study protein adsorption and for biosensing.[20,26,29] The increased surface roughness using GLAD with increased fibronectin adsorption and a decrease in the proliferation of human fibroblasts was reported.[28] In this study, we combined these economical, versatile, and facile techniques to generate ordered nanotopographies for stem cell culture. Biocompatible materials, i.e., Ti (titanium) and Ta (tantalum), were chosen as the substrate materials. With its excellent anticorrosion and biocompatibility, Ta is attracting more and more attention.[30,31] However, it has significantly higher elastic modulus and larger mechanical incompatibility with bone tissue that makes it unsuitable for load-bearing implants. Therefore, porous Ta coatings on Ti implants would enhance the biocompatibility and alleviate the mechanical issue of Ta for use as bone tissue, and the results could directly benefit biomaterials and regenerative medicine.

We first found that increasing the feature height or surface roughness using GLAD inhibited cell spreading, but not cell attachment density and growth of hADSCs. Cell morphology and spreading is one of the first and most obvious parameters to study in the context of the initial cell response to biomaterials. Phenomena called "contact guidance" are quite obvious and straightforward which has been widely recognized and used in biomimetic applications. Although cell−surface interactions are cell-type- and surface-roughness-dependent,[32,33] cells in general do not like rough surfaces and change their shape accordingly. Cells have smaller spreading areas, lesser focal adhesions, and weaker adhesion forces when they

DOI: 10.1021/acsami.5b00107
ACS Appl. Mater. Interfaces 2015, 7, 4979−4989

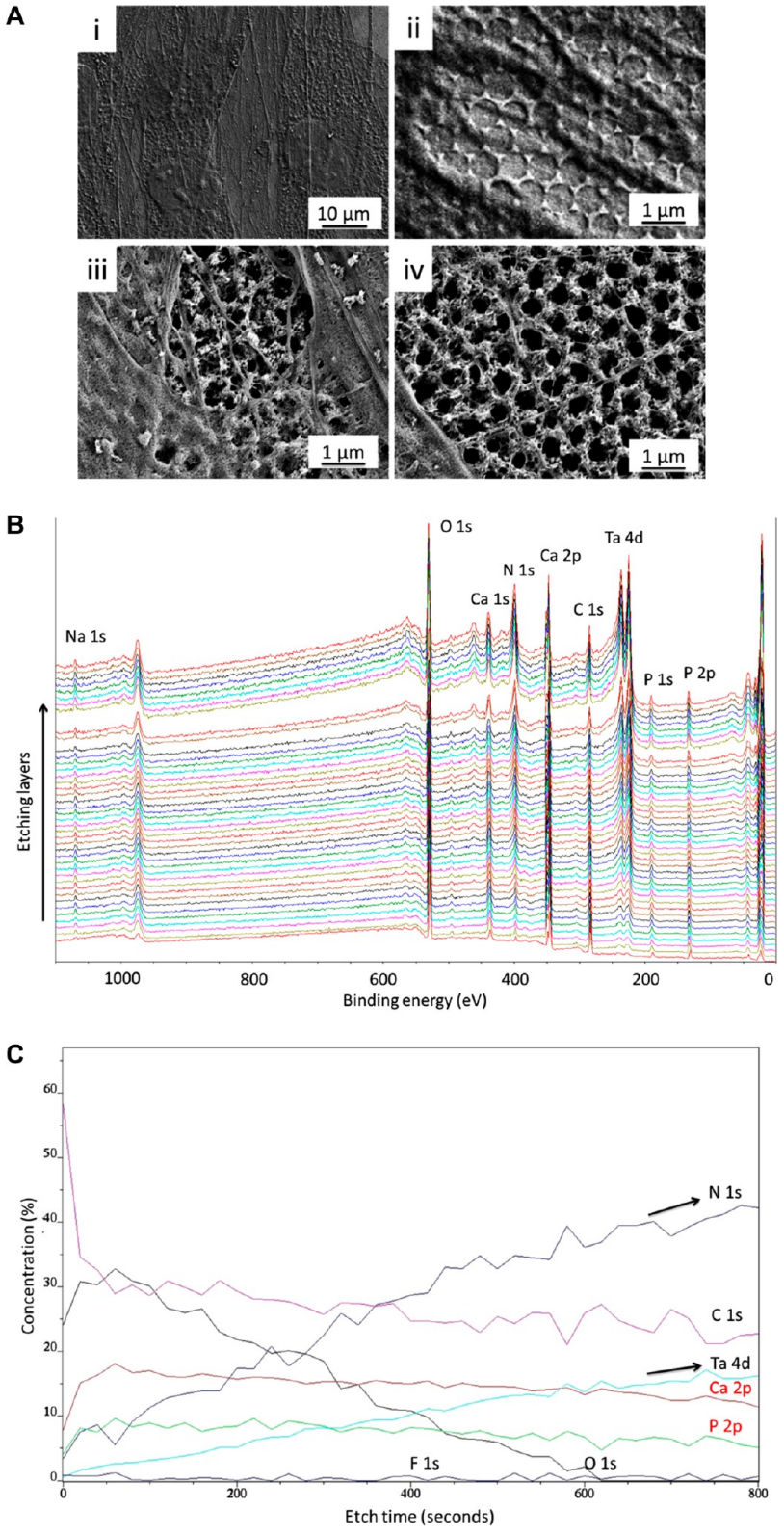

Figure 8. (A) Scanning electron micrographs (SEMs) of hADSCs on surfaces after 2-week osteogenic differentiation. Surface exposure was found on patterned surfaces, especially on (iii) GLAD100 and (iv) GLAD200 surfaces, but not the (i) FLAT surface after long-term culture. There were many extracellular matrix (ECM) deposits on the (iii) GLAD100 and (iv) GLAD200 surfaces, whereas there were lesser ECM deposit found on the (ii) Ta60 and (i) FLAT surfaces. (B) X-ray photoelectron spectroscopy (XPS) chemical depth profiling using a nondestructive Ar cluster source. The survey spectrum was used to analyze the surface composition of each layer. Each layer was etched for 20 s and a total etching time of 800 s was used for the depth profile (40 layers) and to determine (C) the element depth distribution on GLAD200. Carbon (C 1s), oxygen (O 1s), calcium (Ca 2p), and phosphorus (P 2p) was decreased, whereas tantalum (Ta 4d) and nitrogen (N 1s) was increased with increasing time/depth.

DOI: 10.1021/acsami.5b00107
ACS Appl. Mater. Interfaces 2015, 7, 4979−4989

see the surface as a rough substrate. However, anchorage-dependent cells need to attach on solid surfaces to survive. Therefore, even if the surface properties are not optimized, cells still tend to adhere, which results in a smaller cell spreading area. The morphology of anchored cells can be affected by subtle surface differences. Focal adhesion directly determines cell morphology, which is affected by the available surface area where cells can form focal adhesions.[34] The minimal distance between two integrin pairs in order to form mature focal adhesion complexes is approximately 75 nm.[34] When the feature spacing is smaller than 75 nm, the mature focal adhesion complexes can be formed over several features. On the contrary, mature focal adhesion complexes cannot be formed when the feature spacing larger than 75 nm with small or rough features.[32] The disconnection (pore size) of the GLAD samples is approximately 350−400 nm, which is sufficient to inhibit the focal adhesion formation and alter filopodia extension and cell spreading although the overall surface roughness is quite low (Ra ≈ 50 nm). Regarding cell growth, it is a long-term and complex event where cells can express proteins to decorate the surface they attach to. Cells also can adapt to the surface after attachment. Similar trends in initial cell attachment density and growth rates between the surfaces suggest that the overall surface property in this study is not able to inhibit hADSCs adhesion and growth effectively.

We also found, however, that osteogenic differentiation of hADSCs in terms of ALP activity and Ca deposition was stimulated on GLAD surfaces. Previous studies have reported that roughened or textured surfaces might have either positive or negative effects on osteogenic differentiation depending on the surface topography, roughness, material used, and cell types/sources.[32,35−40] Also, there are very few studies focused on different arrangements of nanofeatures (square or hexagonal close-packed) on stem cell differentiation because of the limitations of fabrication. It is therefore difficult to describe a general rule for the topographic effect on osteogenic differentiation and the underlying mechanisms remain unclear. Although the exact signaling mechanisms linking integrin clustering with the commitment of MSC to the osteogenic lineage are essentially unknown, it has been reported that focal adhesion complex formation has a direct effect on the osteogenesis of stem cells when cultured on roughed or textured surfaces.[40,41] The regulation of focal adhesion formation in adherent cells is highly complex and involves both the turnover of single contacts and the reinforcement of the adhesion plaque by protein recruitment. Integrins which mediate signaling between the extracellular matrix (ECM) and the cell interior are crucial in cell survival and differentiation.[42] The major event that triggers osteogenesis is the transition of stem cells into bone-forming differentiated osteoblast cells and is controlled by sequential activation of diverse transcription factors that regulate the expression of specific genes. With reference to focal adhesion-mediated mechanotransduction, integrin-dependent signaling pathways are mediated by non-receptor tyrosine kinases such as focal adhesion kinase (FAK).[43,44] FAK activates downstream extracellular signal-regulated kinase (ERK), which acts as a mediator of cellular differentiation. Activated ERK translocates to the cell nucleus and activates cellular transcription factors to modulate differential functions. It has been shown that translocation of ERK1/2 to the cell nucleus preferentially appeared in cells cultured on topographical features.[45] Except the focal adhesion-related downstream signaling, morphological changes on attached cells also have been reported that affects cell differentiation.[46] Therefore, the influence of nanotopographies on the differentiation of MSCs might be mediated by their effects on the formation of focal adhesions and/or the topography-induced morphological change. Nevertheless, more studies are needed to understand the underlying mechanisms.

Our results also showed that there are visible ECM components deposited on the porous GLAD surfaces after 2 weeks culture. Having higher surface area could be another reason that porous GLAD surfaces can capture and/or retain the produced ECM products on the surfaces compared with Ta60 and FLAT surfaces. hADSCs, which are harvested from human lipoaspirate and therefore make good use of waste material have attracted increased attention recently.[47−49] Several recent reports suggested that nanostructures promote osteogenesis of ADSCs on biomaterial surfaces,[39,50] suggesting that ADSCs are a promising cell source for bone tissue engineering and that the generation of nanostructures on surfaces facilitates osteoblasts-implant integration. Lastly, the effect of surface topography on the differentiation of hADSCs could be minimized when using induction medium because both physical and chemical stimulation are introduced during culture. However, several studies have proved that nano-topographies can stimulate cell differentiation at the gene and protein level without using the induction medium.[1,51] In this study, both induction medium and nanotopographies were used, and the increase in mineralization was demonstrated on GLAD surfaces, suggesting that ordered, porous GLAD nanotopographies facilitate osteogenesis of hADSCs for bone tissue engineering.

5. CONCLUSION

In this study, ordered surface nanostructures have been successfully fabricated on a centimeter-size scale using a combination of colloidal self-assembly, colloidal lithography, and glancing angle deposition (GLAD) techniques. Based on the nature of colloidal self-assembly, surface topographies arranged in a hexagonal close-packed array were produced. The nanostructures had feature sizes ranging from 60 to 200 nm in height, from 13 to 51 nm in Ra roughnesses, and from 81 to 128° in WCA. The behavior of primary human adipose-derived stem cells (hADSCs) was studied on these highly ordered nanostructures. The results showed that ordered nanotopographies inhibited cell spreading, focal adhesion formation and filopodia extension when the GLAD technique was used to increase the surface roughness and feature height. Although the growth rate of cells on each surface was similar, the GLAD surfaces facilitated osteogenic differentiation and ECM component deposition. This study demonstrates that alteration of the feature size of ordered nanotopographies can change stem cell adhesion and differentiation thereby expanding the knowledge in regard to controlling cell−surface interactions, which is of outstanding interest in biomaterials, tissue engineering, and cell therapy applications.

■ ASSOCIATED CONTENT

Supporting Information

(1) Surface topography analysis using atomic force microscopy (Figure S1); (2) Depth profile of surface compositions on GLAD100 using an Ar cluster source and X-ray photoelectron spectroscopy (XPS) (Figure S2). This material is available free of charge via the Internet at http://pubs.acs.org.

DOI: 10.1021/acsami.5b00107
ACS Appl. Mater. Interfaces 2015, 7, 4979−4989

AUTHOR INFORMATION

Corresponding Author

*E-mail: pkingshott@swin.edu.au. Tel: +61 392145033.

Author Contributions

P.Y.W. designed and performed all cell culture experiments and manuscript preparation. D.T.B. performed substrate preparation. M.F. supervised D.T.B. on substrate preparation. T.A. performed the XPS experiments. H.T. and P.K. supervised the project and performed manuscript proofreading.

Notes

The authors declare no competing financial interest.

ACKNOWLEDGMENTS

The Science and Industry Endowment Fund (SIEF) is acknowledged for providing a John Stocker Postdoctoral Research Fellowship for PYW. Part of this work was performed at the Biointerface Engineering Hub at Swinburne part of the Victorian Node of the Australian National Fabrication Facility, a company established under the National Collaborative Research Infrastructure Strategy to provide nano and microfabrication facilities for Australia's researchers.

REFERENCES

(1) Dalby, M. J.; Gadegaard, N.; Tare, R.; Andar, A.; Riehle, M. O.; Herzyk, P.; Wilkinson, C. D.; Oreffo, R. O. The Control of Human Mesenchymal Cell Differentiation Using Nanoscale Symmetry and Disorder. *Nat. Mater.* **2007**, *6*, 997−1003.

(2) Koegler, P.; Clayton, A.; Thissen, H.; Santos, G. N.; Kingshott, P. The Influence of Nanostructured Materials on Biointerfacial Interactions. *Adv. Drug. Delivery Rev.* **2012**, *64*, 1820−39.

(3) Wang, P.-Y.; Yu, J.; Lin, J.-H.; Tsai, W.-B. Modulation of Alignment, Elongation and Contraction of Cardiomyocytes through a Combination of Nanotopography and Rigidity of Substrates. *Acta Biomater.* **2011**, *7*, 3285−3293.

(4) Wang, P.-Y.; Yu, H.-T.; Tsai, W.-B. Modulation of Alignment and Differentiation of Skeletal Myoblasts by Submicron Ridges/Grooves Surface Structure. *Biotechnol. Bioeng.* **2010**, *106*, 285−94.

(5) Dalby, M. J.; Gadegaard, N.; Wilkinson, C. D. The Response of Fibroblasts to Hexagonal Nanotopography Fabricated by Electron Beam Lithography. *J. Biomed. Mater. Res., Part A* **2008**, *84*, 973−9.

(6) Norman, J. J.; Desai, T. A. Methods for Fabrication of Nanoscale Topography for Tissue Engineering Scaffolds. *Ann. Biomed. Eng.* **2006**, *34*, 89−101.

(7) Wood, M. A. Colloidal Lithography and Current Fabrication Techniques Producing in-Plane Nanotopography for Biological Applications. *J. R. Soc. Interface* **2007**, *4*, 1−17.

(8) Li, Y.; Duan, G. T.; Liu, G. Q.; Cai, W. P. Physical Processes-Aided Periodic Micro/Nanostructured Arrays by Colloidal Template Technique: Fabrication and Applications. *Chem. Soc. Rev.* **2013**, *42*, 3614−3627.

(9) Li, Y.; Sasaki, T.; Shimizu, Y.; Koshizaki, N. Hexagonal-Close-Packed, Hierarchical Amorphous TiO_2 Nanocolumn Arrays: Transferability, Enhanced Photocatalytic Activity, and Superamphiphilicity without UV Irradiation. *J. Am. Chem. Soc.* **2008**, *130*, 14755−14762.

(10) Cong, H. L.; Yu, B.; Tang, J. G.; Li, Z. J.; Liu, X. S. Current Status and Future Developments in Preparation and Application of Colloidal Crystals. *Chem. Soc. Rev.* **2013**, *42*, 7774−7800.

(11) Robbie, K.; Brett, M. J.; Lakhtakia, A. Chiral Sculptured Thin Films. *Nature* **1996**, *384*, 616−616.

(12) Zhou, Y.; Taima, T.; Miyadera, T.; Yamanari, T.; Kitamura, M.; Nakatsu, K.; Yoshida, Y. Glancing Angle Deposition of Copper Iodide Nanocrystals for Efficient Organic Photovoltaics. *Nano Lett.* **2012**, *12*, 4146−52.

(13) Summers, M. A.; Brett, M. J. Optimization of Periodic Column Growth in Glancing Angle Deposition for Photonic Crystal Fabrication. *Nanotechnology* **2008**, *19*, 415203.

(14) Kariuki, N. N.; Khudhayer, W. J.; Karabacak, T.; Myers, D. J. Glad Pt-Ni Alloy Nanorods for Oxygen Reduction Reaction. *ACS Catal.* **2013**, *3*, 3123−3132.

(15) Tyagi, M.; Tomar, M.; Gupta, V. Glad Assisted Synthesis of Nio Nanorods for Realization of Enzymatic Reagentless Urea Biosensor. *Biosens. Bioelectron.* **2014**, *52*, 196−201.

(16) Motemani, Y.; Greulich, C.; Khare, C.; Lopian, M.; Buenconsejo, P. J. S.; Schildhauer, T. A.; Ludwig, A.; Koller, M. Adherence of Human Mesenchymal Stem Cells on Ti and TiO_2 Nano-Columnar Surfaces Fabricated by Glancing Angle Sputter Deposition. *Appl. Surf. Sci.* **2014**, *292*, 626−631.

(17) Sengstock, C.; Lopian, M.; Motemani, Y.; Borgmann, A.; Khare, C.; Buenconsejo, P. J.; Schildhauer, T. A.; Ludwig, A.; Koller, M. Structure-Related Antibacterial Activity of a Titanium Nanostructured Surface Fabricated by Glancing Angle Sputter Deposition. *Nanotechnology* **2014**, *25*, 195101.

(18) Pennisi, C. P.; Dolatshahi-Pirouz, A.; Foss, M.; Chevallier, J.; Fink, T.; Zachar, V.; Besenbacher, F.; Yoshida, K. Nanoscale Topography Reduces Fibroblast Growth, Focal Adhesion Size and Migration-Related Gene Expression on Platinum Surfaces. *Colloids Surf., B* **2011**, *85*, 189−197.

(19) Rybczynski, J.; Ebels, U.; Giersig, M. Large-Scale, 2D Arrays of Magnetic Nanoparticles. *Colloid Surface A* **2003**, *219*, 1−6.

(20) Ogaki, R.; Bennetsen, D. T.; Bald, I.; Foss, M. Dopamine-Assisted Rapid Fabrication of Nanoscale Protein Arrays by Colloidal Lithography. *Langmuir* **2012**, *28*, 8594−8599.

(21) Wang, P.-Y.; Li, W.-T.; Yu, J.; Tsai, W.-B. Modulation of Osteogenic, Adipogenic and Myogenic Differentiation of Mesenchymal Stem Cells by Submicron Grooved Topography. *J. Mater. Sci. Mater. Med.* **2012**, *23*, 3015−28.

(22) Wang, P.-Y.; Wu, T.-H.; Chao, P.-H.; Kuo, W.-H.; Wang, M.-J.; Hsu, C.-C.; Tsai, W.-B. Modulation of Cell Attachment and Collagen Production of Anterior Cruciate Ligament Cells Via Submicron Grooves/Ridges Structures with Different Cell Affinity. *Biotechnol. Bioeng.* **2013**, *110*, 327−37.

(23) Biggs, M. J. P.; Richards, R. G.; Gadegaard, N.; McMurray, R. J.; Affrossman, S.; Wilkinson, C. D. W.; Oreffo, R. O. C.; Dalby, M. J. Interactions with Nanoscale Topography: Adhesion Quantification and Signal Transduction in Cells of Osteogenic and Multipotent Lineage. *J. Biomed. Mater. Res., Part A* **2009**, *91*, 195−208.

(24) Hajati, S.; Tougaard, S. XPS for Non-Destructive Depth Profiling and 3D Imaging of Surface Nanostructures. *Anal. Bioanal. Chem.* **2010**, *396*, 2741−2755.

(25) Li, Y.; Koshizaki, N.; Wang, H.; Shimizu, Y. Untraditional Approach to Complex Hierarchical Periodic Arrays with Ternary Stepwise Architectures of Micro-, Submicro-, and Nanosized Structures Based on Binary Colloidal Crystals and Their Fine Structure Enhanced Properties. *ACS Nano* **2011**, *5*, 9403−12.

(26) Ye, X. Z.; Qi, L. M. Two-Dimensionally Patterned Nanostructures Based on Monolayer Colloidal Crystals: Controllable Fabrication, Assembly, and Applications. *Nano Today* **2011**, *6*, 608−631.

(27) Wang, P.-Y.; Wu, T.-H.; Tsai, W.-B.; Kuo, W.-H.; Wang, M.-J. Grooved Plga Films Incorporated with Rgd/Yigsr Peptides for Potential Application on Skeletal Muscle Tissue Engineering. *Colloids Surf., B* **2013**, *110*, 88−95.

(28) Dolatshahi-Pirouz, A.; Pennisi, C. P.; Skeldal, S.; Foss, M.; Chevallier, J.; Zachar, V.; Andreasen, P.; Yoshida, K.; Besenbacher, F. The Influence of Glancing Angle Deposited Nano-Rough Platinum Surfaces on the Adsorption of Fibrinogen and the Proliferation of Primary Human Fibroblasts. *Nanotechnology* **2009**, *20*, 095101.

(29) Singh, G.; Gohri, V.; Pillai, S.; Arpanaei, A.; Foss, M.; Kingshott, P. Large-Area Protein Patterns Generated by Ordered Binary Colloidal Assemblies as Templates. *ACS Nano* **2011**, *5*, 3542−3551.

(30) Tang, Z.; Xie, Y.; Yang, F.; Huang, Y.; Wang, C.; Dai, K.; Zheng, X.; Zhang, X. Porous Tantalum Coatings Prepared by Vacuum Plasma Spraying Enhance BMSCs Osteogenic Differentiation and Bone Regeneration in Vitro and in Vivo. *PloS one* **2013**, *8*, e66263.

DOI: 10.1021/acsami.5b00107
ACS Appl. Mater. Interfaces 2015, 7, 4979−4989

(31) Wang, N.; Li, H.; Wang, J.; Chen, S.; Ma, Y.; Zhang, Z. Study on the Anticorrosion, Biocompatibility, and Osteoinductivity of Tantalum Decorated with Tantalum Oxide Nanotube Array Films. *ACS Appl. Mater. Interfaces* **2012**, *4*, 4516−23.
(32) Wang, P.-Y.; Clements, L. R.; Thissen, H.; Jane, A.; Tsai, W.-B.; Voelcker, N. H. Screening Mesenchymal Stem Cell Attachment and Differentiation on Porous Silicon Gradients. *Adv. Funct. Mater.* **2012**, *22*, 3414−3423.
(33) Wang, P.-Y.; Clements, L. R.; Thissen, H.; Hung, S.-C.; Cheng, N.-C.; Tsai, W.-B.; Voelcker, N. H. Screening the Attachment and Spreading of Bone Marrow-Derived and Adipose-Derived Mesenchymal Stem Cells on Porous Silicon Gradients. *RSC Adv.* **2012**, *2*, 12857−12865.
(34) Lamers, E.; van Horssen, R.; te Riet, J.; van Delft, F. C.; Luttge, R.; Walboomers, X. F.; Jansen, J. A. The Influence of Nanoscale Topographical Cues on Initial Osteoblast Morphology and Migration. *Eur. Cell Mater.* **2010**, *20*, 329−43.
(35) Schneider, G. B.; Zaharias, R.; Seabold, D.; Keller, J.; Stanford, C. Differentiation of Preosteoblasts is Affected by Implant Surface Microtopographies. *J. Biomed. Mater. Res., Part A* **2004**, *69*, 462−468.
(36) Matsuzaka, K.; Walboomers, X. F.; Yoshinari, M.; Inoue, T.; Jansen, J. A. The Attachment and Growth Behavior of Osteoblast-Like Cells on Microtextured Surfaces. *Biomaterials* **2003**, *24*, 2711−9.
(37) Biggs, M. J.; Richards, R. G.; Gadegaard, N.; Wilkinson, C. D.; Oreffo, R. O.; Dalby, M. J. The Use of Nanoscale Topography to Modulate the Dynamics of Adhesion Formation in Primary Osteoblasts and Erk/Mapk Signalling in Stro-1+ Enriched Skeletal Stem Cells. *Biomaterials* **2009**, *30*, 5094−103.
(38) Kirmizidis, G.; Birch, M. A. Microfabricated Grooved Substrates Influence Cell-Cell Communication and Osteoblast Differentiation in Vitro. *Tissue Eng., Part A* **2009**, *15*, 1427−36.
(39) Xia, L.; Lin, K.; Jiang, X.; Fang, B.; Xu, Y.; Liu, J.; Zeng, D.; Zhang, M.; Zhang, X.; Chang, J.; Zhang, Z. Effect of Nano-Structured Bioceramic Surface on Osteogenic Differentiation of Adipose Derived Stem Cells. *Biomaterials* **2014**, *35*, 8514−27.
(40) Biggs, M. J. P.; Dalby, M. J. Focal Adhesions in Osteoneogenesis. *Proc. Inst. Mech. Eng., Part H* **2010**, *224*, 1441−1453.
(41) Yim, E. K.; Darling, E. M.; Kulangara, K.; Guilak, F.; Leong, K. W. Nanotopography-Induced Changes in Focal Adhesions, Cytoskeletal Organization, and Mechanical Properties of Human Mesenchymal Stem Cells. *Biomaterials* **2010**, *31*, 1299−306.
(42) Grigoriou, V.; Shapiro, I. M.; Cavalcanti-Adam, E. A.; Composto, R. J.; Ducheyne, P.; Adams, C. S. Apoptosis and Survival of Osteoblast-Like Cells Are Regulated by Surface Attachment. *J. Biol. Chem.* **2005**, *280*, 1733−9.
(43) Schaller, M. D.; Borgman, C. A.; Cobb, B. S.; Vines, R. R.; Reynolds, A. B.; Parsons, J. T. Pp125fak a Structurally Distinctive Protein-Tyrosine Kinase Associated with Focal Adhesions. *Proc. Natl. Acad. Sci. U.S.A.* **1992**, *89*, 5192−6.
(44) Hamilton, D. W.; Brunette, D. M. The Effect of Substratum Topography on Osteoblast Adhesion Mediated Signal Transduction and Phosphorylation. *Biomaterials* **2007**, *28*, 1806−19.
(45) Kokubu, E.; Hamilton, D. W.; Inoue, T.; Brunette, D. M. Modulation of Human Gingival Fibroblast Adhesion, Morphology, Tyrosine Phosphorylation, and Erk 1/2 Localization on Polished, Grooved and Sla Substratum Topographies. *J. Biomed. Mater. Res., Part A* **2009**, *91*, 663−70.
(46) Tsimbouri, P.; Gadegaard, N.; Burgess, K.; White, K.; Reynolds, P.; Herzyk, P.; Oreffo, R.; Dalby, M. J. Nanotopographical Effects on Mesenchymal Stem Cell Morphology and Phenotype. *J. Cell Biochem.* **2014**, *115*, 380−90.
(47) Arnalich-Montiel, F.; Pastor, S.; Blazquez-Martinez, A.; Fernandez-Delgado, J.; Nistal, M.; Alio, J. L.; De Miguel, M. P. Adipose-Derived Stem Cells Are a Source for Cell Therapy of the Corneal Stroma. *Stem Cells* **2008**, *26*, 570−9.
(48) Ruetze, M.; Richter, W. Adipose-Derived Stromal Cells for Osteoarticular Repair: Trophic Function Versus Stem Cell Activity. *Expert. Rev. Mol. Med.* **2014**, *16*, e9.
(49) Wu, L.; Cai, X. X.; Zhang, S.; Karperien, M.; Lin, Y. F. Regeneration of Articular Cartilage by Adipose Tissue Derived Mesenchymal Stem Cells: Perspectives from Stem Cell Biology and Molecular Medicine. *J. Cell Physiol.* **2013**, *228*, 938−944.
(50) Liu, J.; Wang, X.; Jin, Q.; Jin, T.; Chang, S.; Zhang, Z.; Czajka-Jakubowska, A.; Giannobile, W. V.; Nor, J. E.; Clarkson, B. H. The Stimulation of Adipose-Derived Stem Cell Differentiation and Mineralization by Ordered Rod-Like Fluorapatite Coatings. *Biomaterials* **2012**, *33*, 5036−46.
(51) Dalby, M. J.; Andar, A.; Nag, A.; Affrossman, S.; Tare, R.; McFarlane, S.; Oreffo, R. O. C. Genomic Expression of Mesenchymal Stem Cells to Altered Nanoscale Topographies. *J. R. Soc. Interface* **2008**, *5*, 1055−1065.
(52) Wang, P.-Y.; Pingle, H.; Koegler, P.; Thissen, H.; Kingshott, P. *J. Mater. Chem. B* **2015**, DOI: 10.1039/c4tb02006e.

DOI: 10.1021/acsami.5b00107
ACS Appl. Mater. Interfaces 2015, 7, 4979−4989